



A magnetic separation method for isolating and characterizing the biomolecular corona of lipid nanoparticles

Valentina Francia^{a,b,1,2} , Yao Zhang^{a,1}, Miffy Hok Yan Cheng^a, Raymond M. Schifflers^b, Dominik Witzigmann^{a,c}, and Pieter R. Cullis^{a,c,2}

Edited by James Dahlman, Emory University, Atlanta, GA; received June 19, 2023; accepted September 22, 2023 by Editorial Board Member Christine E. Seidman

Lipid nanoparticle (LNP) formulations are a proven method for the delivery of nucleic acids for gene therapy as exemplified by the worldwide rollout of LNP-based RNAi therapeutics and mRNA vaccines. However, targeting specific tissues or cells is still a major challenge. After LNP administration, LNPs interact with biological fluids (i.e., blood), components of which adsorb onto the LNP surface forming a layer of biomolecules termed the “biomolecular corona (BMC)” which affects LNP stability, biodistribution, and tissue tropism. The mechanisms by which the BMC influences tissue- and cell-specific targeting remains largely unknown, due to the technical challenges in isolating LNPs and their corona from complex biological media. In this study, we present a new technique that utilizes magnetic LNPs to isolate LNP–corona complexes from unbound proteins present in human serum. First, we developed a magnetic LNP formulation, containing >40 superparamagnetic iron oxide nanoparticles (IONPs)/LNP, the resulting LNPs containing iron oxide nanoparticles (IOLNPs) displayed a similar particle size and morphology as LNPs loaded with nucleic acids. We further demonstrated the isolation of the IOLNPs and their corresponding BMC from unbound proteins using a magnetic separation (MS) system. The BMC profile of LNP from the MS system was compared to size exclusion column chromatography and further analyzed via mass spectrometry, revealing differences in protein abundances. This new approach enabled a mild and versatile isolation of LNPs and its corona, while maintaining its structural integrity. The identification of the BMC associated with an intact LNP provides further insight into LNP interactions with biological fluids.

lipid nanoparticles | iron oxide nanoparticles | biomolecular corona | magnetic separation

Lipid nanoparticles (LNP) have emerged as an effective nonviral delivery system for nucleic acid payloads due to their high encapsulation efficiency, low toxicity, ability to facilitate intracellular delivery, and the possibility to modulate their size and surface properties (1–3). The technological advances carried out in the past three decades have enabled the clinical approval of the first LNP-based siRNA therapeutic, Onpatro (4–6), which quickly became a landmark formulation that paved the way for the widespread use of LNP as nucleic acid delivery systems (2, 7, 8) and for the worldwide rollout of the LNP-based vaccines against SARS-CoV-2 (9).

However, like many other nanomedicines, LNP suffer from a low selectivity and specificity for target cells and organs and limits clinical translation (10, 11). First of all, nanoparticles can be rapidly sequestered by macrophages into the liver and other secondary lymphoid organs, which impair their delivery to target tissues (12). Moreover, while ligand-targeted nanomedicines show a higher efficacy *in vitro* compared to their untargeted counterpart, this advantage is often lost *in vivo* due to masking from the formation of a biomolecular protein corona (BMC) (13). The formation of a BMC can be an advantage as several groups have shown that once *i.v.* administered, the BMC could enable LNPs to possess extrinsic targeting properties, directing them towards specific cell receptors (14–18). An early example of this includes Onpatro, as its ability to interact with specific serum proteins (Apolipoprotein E) after *i.v.* administrations, directs the LNP towards low-density lipoprotein receptors on the surface of hepatocytes (5, 6, 19). More recently, studies have focused on extrahepatic delivery by optimizing the physiochemical properties of LNPs to drive distinct BMC profiles, subsequently, enabling targeting of nonliver organs such as the spleen or lungs (20–22). For example, in the context of an LNP–mRNA vaccine, it is advantageous for LNPs to have a favourable corona for targeting and transfecting immune cells in lymphatic organs to induce an effective immune response. Yet, achieving extrahepatic delivery still remains a challenging topic within the field due to the lack of understanding between the nano–bio relationship. This “passive” targeting specificity underlines the importance of studying in depth the biological interactions that occur at the LNP surface to allow us to predict and modulate LNP’s fate, biodistribution, and targeting.

Significance

Lipid nanoparticle (LNP) technology is increasingly enabling many gene therapies. Once LNPs are administered *in vivo*, preferential LNP targeting to desired cells can be attributed to the formation of a biomolecular corona (BMC), however, characterization of the corona is challenging. This is due to poor separation efficiency of LNP–corona complexes from unbound proteins. Herein, we developed magnetic iron-oxide-loaded LNPs (IOLNP) that allow separation of LNP–corona complexes from biological media through magnetic separation. This technology enables a rapid and selective method to separate LNP–corona complexes and enables in-depth characterization of the BMC while maintaining the particle integrity.

Author contributions: V.F., Y.Z., R.M.S., D.W., and P.R.C. designed research; V.F., Y.Z., and M.H.Y.C. performed research; V.F., Y.Z., and P.R.C. contributed new reagents/analytic tools; V.F., Y.Z., M.H.Y.C., R.M.S., D.W., and P.R.C. analyzed data; and V.F., Y.Z., M.H.Y.C., and P.R.C. wrote the paper.

Competing interest statement: P.R.C. and D.W. have financial interests in NanoVation Therapeutics. D.W. is an employee of NanoVation Therapeutics.

This article is a PNAS Direct Submission. J.D. is a guest editor invited by the Editorial Board.

Copyright © 2024 the Author(s). Published by PNAS. This open access article is distributed under [Creative Commons Attribution-NonCommercial-NoDerivatives License 4.0 \(CC BY-NC-ND\)](https://creativecommons.org/licenses/by-nc-nd/4.0/).

¹V.F. and Y.Z. contributed equally to this work.

²To whom correspondence may be addressed. Email: valentina.francia01@gmail.com or pieterc@ubc.mail.ca.

This article contains supporting information online at <https://www.pnas.org/lookup/suppl/doi:10.1073/pnas.2307803120/-/DCSupplemental>.

Published March 4, 2024.

To systematically study the LNPs and their newly formed corona, the unbound proteins must be separated after their in vivo administration or in vitro incubation with blood, plasma, or serum. However, a precise characterization of the BMC of soft nanomaterials, such as LNPs has proven difficult as the size and density of LNPs are similar to “natural” serum nanoparticles, for instance, chylomicrons, HDL, exosomes, and many more (19).

Common separation techniques such as size exclusion chromatography (SEC) or (ultra)centrifugation are based on, respectively, size or density, and therefore they can work well for the study of bigger or dense NPs (23) but do not allow an effective separation of LNP (30 to 100 nm) from lipoproteins and related nanostructures (7 to 80 nm) present in biological media (19). In addition, as a high g-force is commonly required in (ultra)centrifugation, proteins and LNP can aggregate and induce artifacts resulting in difficulty differentiating between unbound vs. adsorbed proteins. The lack of effective and high-throughput separation techniques for soft nanomaterials has led to alternative procedures such as cross-linking proteins on the LNP surface (24, 25). This effectively removes the presence of unbounded proteins but potentially disrupts the proteins present on an intact LNP surface. Furthermore, a photoaffinity lipid probe is required in the LNP formulation which can also alter the BMC formation and profile due to deviations from clinically relevant lipid compositions. In some cases, affinity assays have been used for isolating the corona of PEGylated nanomedicines (26). However, since many affinity-based assays rely on ligand binding to the polyethylene glycol (PEG) lipid, LNPs that contains diffusible PEG that are engineered to shed from the particle surface (i.e., Onpattro) may not be suitable for this method.

In this work, we demonstrate a magnetic separation (MS) technique that enables the study of LNP's BMC in a manner that is independent of their surface properties. This technique is rapid and amenable to high-throughput applications. To accomplish this, we encapsulate 5-nm hydrophilic iron oxide nanoparticles, which have superparamagnetic properties, in the core of an Onpattro-like LNP formulation. We show that these iron oxide LNP (IOLNP) can be retained on a column incorporating high magnetic field gradients, allowing separation of IOLNP from serum after incubation in human serum, while preserving the LNP's corona and particle integrity. Using a clinically relevant LNP lipid composition, this method allowed us to identify a unique BMC profile, which differed from that achieved by other conventional methods such as SEC.

Results

Optimization and Enrichment of Iron-Oxide Encapsulated LNP (IOLNP). First, IOLNP were formulated using an Onpattro-based lipid composition (with the inclusion of a lipophilic fluorescent dye) and molar ratio containing 50.0/10.0/38.5/1.5/0.5 of DLin-MC3-DMA/DSPC/Cholesterol/PEG-DMG/DiDC18 using a T-tube mixing method as described by Leung et al. (27) We investigated the encapsulation of IONPs in LNP by titrating the concentration of IONPs (1.1×10^{13} to 8.8×10^{13} IONPs/ μmol lipids) added to the aqueous mix using a method adapted from the encapsulation process of gold nanoparticles by Bromma et al. (28). Four stock IOLNP formulations were prepared (Table 1 and *SI Appendix, Table S1*). The formulations were purified and enriched through a magnetic separator containing a magnetic column as summarized in Fig. 1A. Increasing the IONP concentration to lipid ratio in the formulation resulted in an increased recovery rate after MS (38% lipid recovery) as shown in formulation D (Fig. 1B). For all formulations, cryo-TEM images

Table 1. IOLNP were formulated as described in the Materials and Methods, using an increasing concentration of IONPs/ μmol lipids and then imaged via cryo-TEM

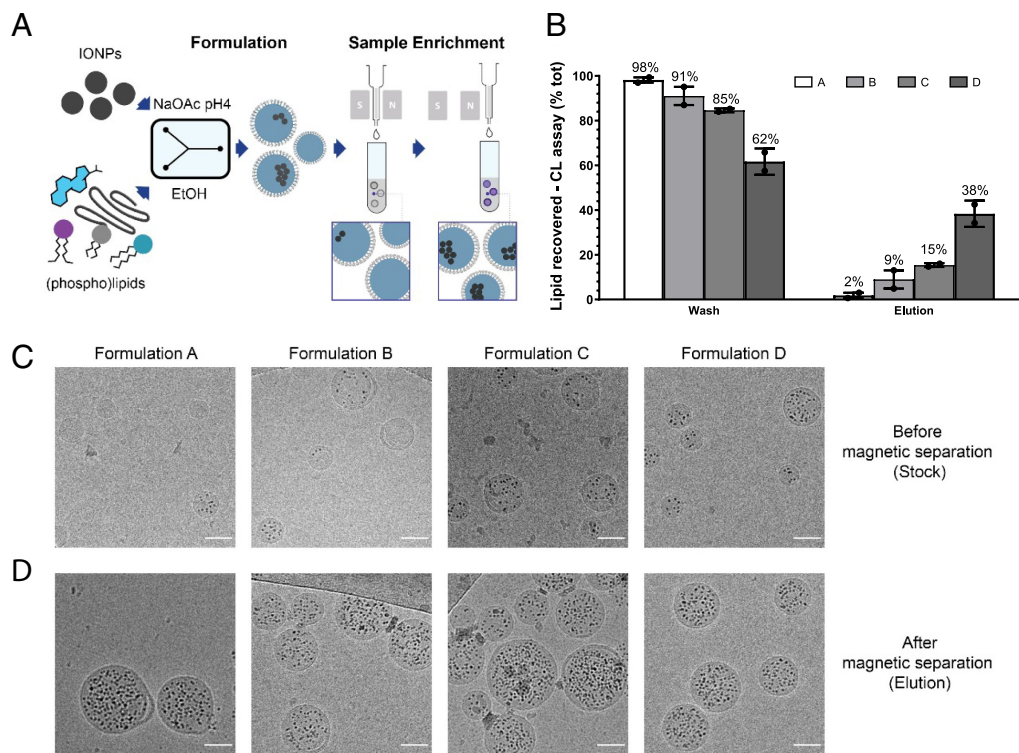
Formulation	A	B	C	D
IONPs/ μmol lipids	1.1×10^{13}	2.2×10^{13}	4.4×10^{13}	8.8×10^{13}
LNP \emptyset (Cryo-TEM)	41.8 ± 8.2	51.4 ± 11.7	49.5 ± 14.2	47.5 ± 12.5
Number IONPs/ LNP	2.3 ± 4.6	6.4 ± 6.7	9.7 ± 8.7	12.7 ± 11.9

The average diameter (\emptyset) and average number of encapsulated IONP (IONP/LNP) of $n = 100$ randomly selected IOLNPs were measured manually using the Fiji software and reported in the table with their SDs. By increasing IONP concentration, the number of IONP per particle (IONP/LNP) increased as well.

show the presence of empty LNPs (without IONPs) or LNPs with a variable number of encapsulated electron-dense IONPs per particle (Fig. 1C). IONPs encapsulation produces LNPs with a “solid core” structure in agreement with that reported for the standard Onpattro formulation (29) and in line with previous observations for encapsulated gold nanomaterials (28). Overall, all four stock formulations had the same average diameter, while formulation D resulted in the highest number of IONP encapsulated (12.7 ± 11.9) (Table 1). To further enrich IOLNP, the four formulations were loaded into a magnetic column. The column allowed the removal of empty or insufficiently IONP-loaded LNP (wash) while retaining the highly magnetic IOLNP. The magnetic separator was then removed and magnetic IOLNP retained were subsequently eluted. For all four IONP concentrations tested, the particle size in the elution fraction was higher than the stock suggesting fractionation of the IOLNPs (*SI Appendix, Fig. S1*). This is also evident in cryo-TEM images which show the resulting eluted samples were enriched in LNPs containing IONPs in their core (Fig. 1D). Consequently, formulation D was selected for further investigations.

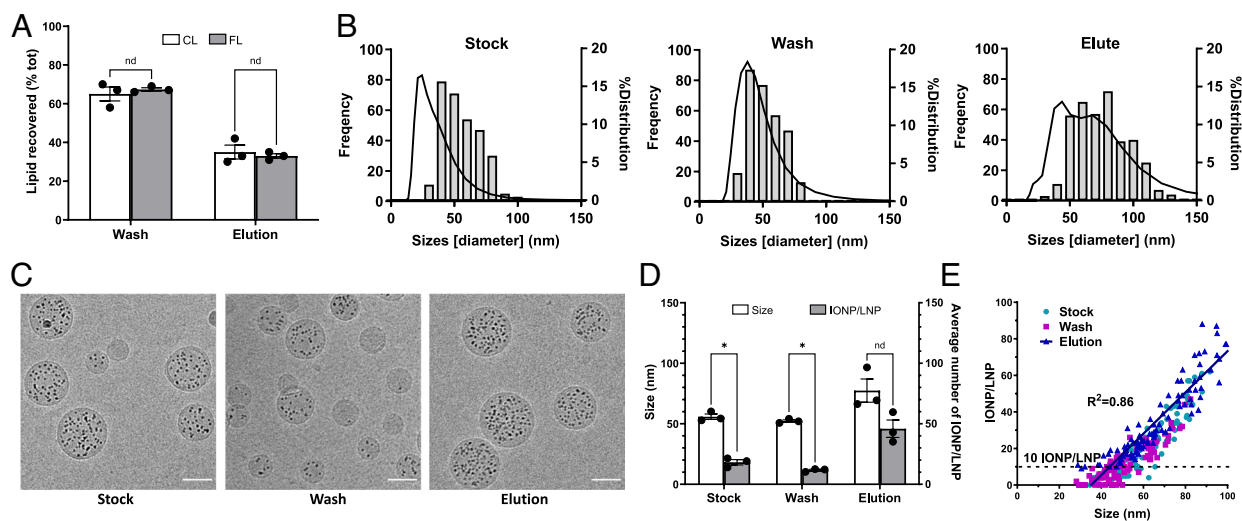
Characterization of IOLNP Fractions and the MS Method. After optimizing IOLNP formulations, Formulation D was used to select the best commercially available magnetic column that could allow the highest recovery before further experiments were conducted (*SI Appendix, Fig. S1*). Column LD was selected as it yields the most efficient separation and retention of IOLNP. Next, we further characterized the different LNP fractions collected from the MS method. Both cholesterol and fluorescence assays confirmed a $\sim 35\%$ IOLNP recovery rate after MS (Fig. 2A). To assess whether the recovery rate was due to the particle properties and not to the fact that the column could retain fixed amounts of sample and evaluate the reproducibility of this technique, the elution fraction was run through another column a second time. Then, 96% of all recovered particles were found in the elution fraction (*SI Appendix, Fig. S2*) confirming the validity of this technique.

DLS measurement and cryo-TEM images confirmed nanoparticle sizes and IONPs encapsulation efficacy in the collected fractions (Fig. 2B and C and *SI Appendix, Table S2*). DLS revealed the particle size distribution for wash and eluted LNPs that is in concordance to the size distribution observed in cryo-TEM images. A discrepancy in the LNPs diameter measured by DLS and cryo-TEM was observed for the stock LNPs and this can be attributed to the unencapsulated and aggregated IONP in the stock solution prior to magnetic column chromatography purification (*SI Appendix, Fig. S3A*). It was observed that the stock sample contains a mix of empty/small IOLNP and loaded/big IOLNP and has a lower diameter (56 nm) and a lower amount of encapsulated IONPs/LNP (18 IONPs/LNP) compared to the elution fraction. The eluted IOLNP fraction had the highest diameter (77 nm) and the highest number



of encapsulated IONPs (46 IONPs/LNP) (Fig. 2D and *SI Appendix, Fig. S3C*). Overall, a linear correlation between LNP diameter and the amount of encapsulated IONP was observed, with bigger particles containing the highest number of IONPs. The minimum number of IONP encapsulated that allowed IOLNP retention into the magnet was calculated to be approximately 10 IONPs/LNP as

only LNP containing more than 10 IONP were found in the elution fraction (Fig. 2E and *SI Appendix, Fig. S3 B and C*). To verify the effective separation between IOLNP vs. nonencapsulated IONPs, nonencapsulated free IONPs were passed through the magnetic column, where most IONPs flowed through with low retention to the column (*SI Appendix, Fig. S4*). Cryo-TEM analysis



Downloaded from https://www.pnas.org by 128.189.94.166 on June 10, 2024 from IP address 128.189.94.166.

of the wash and elution fractions of IOLNPs indicated that majority of the free IONP are removed from the wash fraction (77.7%), with only 22.3% free IONP remaining in the elution fraction upon column purification (*SI Appendix, Fig. S3D*). Therefore, we were able to confirm that the first MS step allowed purification of stock sample and yielded IOLNP samples uniform in size, number of encapsulated IONP, and magnetic properties, while effectively removing the majority of nonencapsulated IONP from the sample.

Separation and Analysis of the BMC-LNP Complex. To adsorb a BMC to our LNP formulation, the optimized and enriched formulation D was incubated in human serum at 37 °C for 1 h, following the method used by Hadjidemetriou et al. (30). To form a representative LNP surface to serum ratio, we used the same lipid concentration (94 μg total lipids in 1 mL human serum) used clinically for Onpatro (0.3 mg siRNA per kg or 3.3 mg of total lipids per kg). It is important to note that the LNP/serum ratio used in this study is much lower than the one used during in standard in vitro experiments (which normally use 10% serum

and higher LNP concentrations) in order to better reflect the biological interactions in vivo.

To compare the outcomes of the current method with established techniques, MS was performed in parallel with studies using SEC, a well-established technique for this type of study (Fig. 3*A*) (19, 23, 31, 32). The same sample containing LNPs, their corona, and free proteins and lipoproteins, was used for both MS or SEC method. Samples from the collected elution fraction from each method were analyzed by cryo-TEM and compared (Fig. 3*B*). Abundant vesicles (white arrows), showed a similar size and morphology to lipoproteins (33), could be observed in the SEC sample, while the MS sample contained few of those structures. This observation indicates that free lipoproteins present in human serum were more efficiently removed with MS. Next, the protein size and population in the recovered eluted samples were further analyzed through polyacrylamide gel electrophoresis (PAGE) (Fig. 3*C* and *SI Appendix, Fig. S5*). Much different protein profiles were observed between MS and SEC as indicated by the PAGE analysis, the only proteins common to both techniques were observed around 25 kDa and 60 to 75 kDa. The lipid concentration measured by

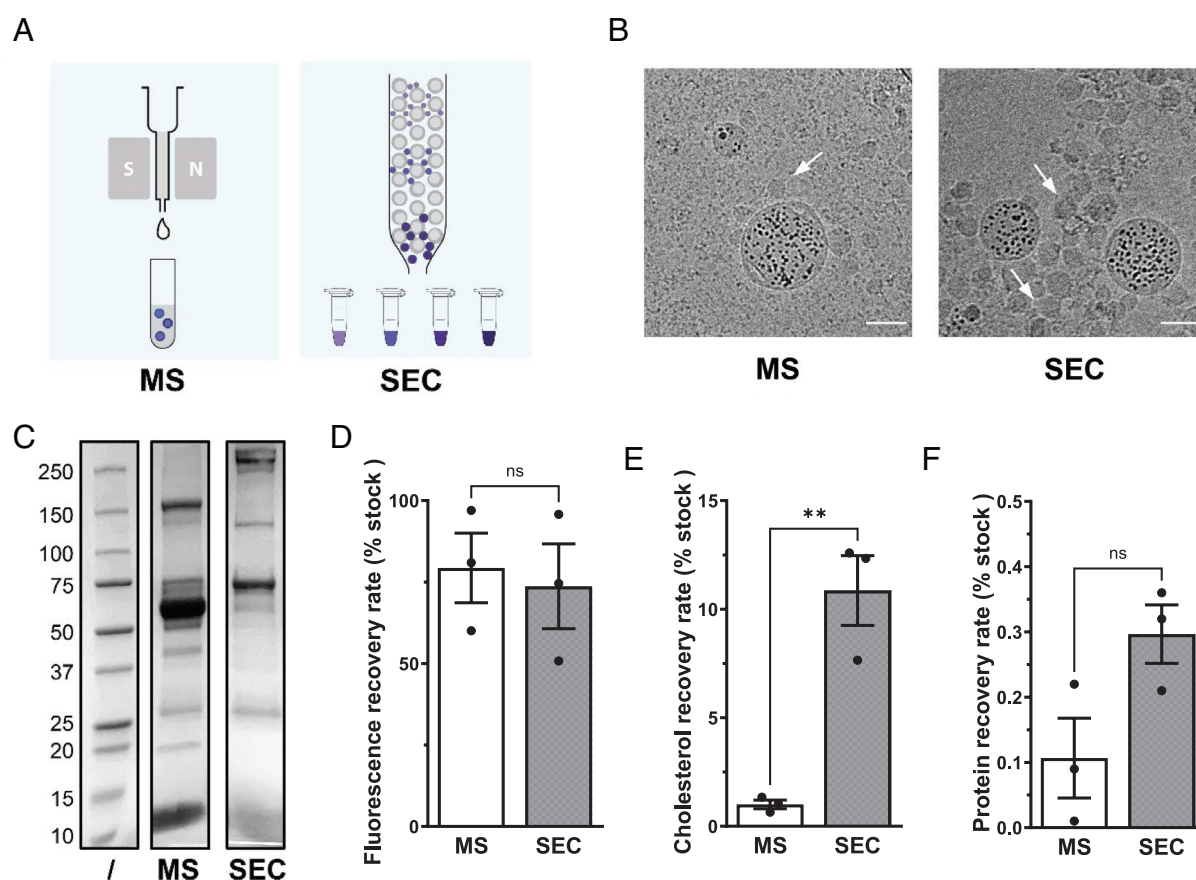


Fig. 3. IOLNP–corona complexes isolation by MS and SEC. IOLNPs were formulated and enriched in IONP-loaded LNPs as described in the *Materials and Methods*. The enriched IOLNPs were incubated in human serum for 1 h at 37 °C and then 1 mL of human serum and IOLNPs was run through a magnetic (MS) or a SEC column. For MS, the elution fraction was collected and analyzed. For SEC, the eluted fractions were collected, and then only fractions containing fluorescent IOLNPs were merged and analyzed. (A) Schematics of the two techniques. (B) Cryo-TEM micrographs of the MS elution fraction and the SEC merged fractions. In the sample separated by SEC, we can clearly distinguish vesicles (lipoproteins) derived from human serum (white arrows), which are almost totally absent in the samples separated by MS. (Scale bar, 50 nm.) (C) Representative image showing the protein profile of samples isolated by MS or SEC. The protein content of the two samples was quantified, then the samples were loaded into a polyacrylamide gel and stained with Coomassie blue. (D) IOLNP recovery rate was measured by comparing the fluorescence signal of the eluates and the stock solution of IOLNPs in human serum. The signal is very similar in both samples, indicating that a similar amount of LNPs has been recovered with the two separation methods (around 80% of stock IOLNPs). Data were analyzed through a two-tailed unpaired *t* test, ns: nonsignificance. (E) Cholesterol content of the recovered fractions were measured by Cholesterol E assay and reported here as average and SE of three independent experiments. Cholesterol recovery (left y axis) is less than 1% of the stock for the MS sample, while it is more than 10% for the SEC sample, indicating that the latter contains more lipoproteins. Data were analyzed through a two-tailed unpaired *t* test, $**P < 0.01$. (F) Protein contents of the recovered fractions were measured by BCA assay and reported here as average and SE of three independent experiments. Data were analyzed through a two-tailed unpaired *t* test, ns: nonsignificance.

fluorescence also indicated that about 80% of the initial IOLNPs dose was recovered after separation with both techniques (Fig. 3D). However, protein and cholesterol assays show that samples separated by SEC contained more protein and 10 times more cholesterol than samples separated by MS (Fig. 3E and F). This indicates, once again, that the MS method improves separation and removal of unbound proteins. It should be noted that the magnetic column does not elicit any serum protein biases (SI Appendix, Fig. S5C).

Identification of the Adsorbed Proteins in the BMC. Isolated LNP–corona complexes and their adsorbed protein composition were further analyzed by liquid chromatography–mass spectrometry (LC–MS). More than 200 proteins were identified for each sample. The heatmap showed a different protein abundance between the SEC and MS samples (represented with a cyan to orange color code) (Fig. 4A), where 25% of the proteins analyzed (50 out of 200) were significantly different. These include proteins such as Fetuin-A (FETUA), a glycoprotein expressed in hepatocytes, and plays a role in promoting endocytosis (34), showing higher abundance in MS over SEC. These differences were explored more in detail by performing a *t* test (Fig. 4B). Only significant values (above the black lines) were considered. Overall, up to 50 significantly different proteins between the two conditions were identified, with the top 10 shown in Fig. 4C. Interestingly, MS samples are enriched in complement factors compared to SEC samples. Although common serum proteins including apolipoprotein E, apolipoprotein AI, and albumin were present in both separation methods, the mass spectrometry results highlight the impact different isolation method can have on the variability when studying the BMC composition. This clearly indicates the use of more effective and reliable separation strategies of an

intact LNP against unbound proteins can reveal new structural information and insight toward the LNP–corona complexes.

Discussion

We have developed a new type of magnetic LNP as a model for using MS to study the BMC of LNPs. We have established an experimental workflow that is highly versatile for the isolation of an intact LNP with the adsorbed protein corona as shown in Scheme 1.

Common BMC separation techniques such as centrifugation have previously been implemented for identifying enriched proteins adsorbed on the surface of LNPs (21, 22), however, the harsh separation process required likely affected the LNP integrity during pellet formation and may not effectively remove unbound proteins (35). This MS method offers distinct advantages over conventional methods, such as the ability to use LNP formulation containing the same molar ratio and lipid composition as clinically relevant formulations while recovering isolated intact LNP–corona samples with lower amounts of unwanted free proteins. However, like most LNP–corona separation techniques, there are also limitations to the MS method. The IONP encapsulation process will need to be reoptimized for formulations containing different molar ratios of the ionizable lipid as the separation efficiency is expected to be positively correlated with the amount of ionizable lipid present. For example, lowering the ionizable lipid content in LNP formulations will likely lower the number of IONPs/LNP as there will be fewer protonated ionizable lipid molecules to complex with the negatively charged IONPs when formulating at low pH. However, because the MS method relies on material encapsulated in the core of the LNP, rather than isolation methods that depend on changing the surface properties, we suggest that the

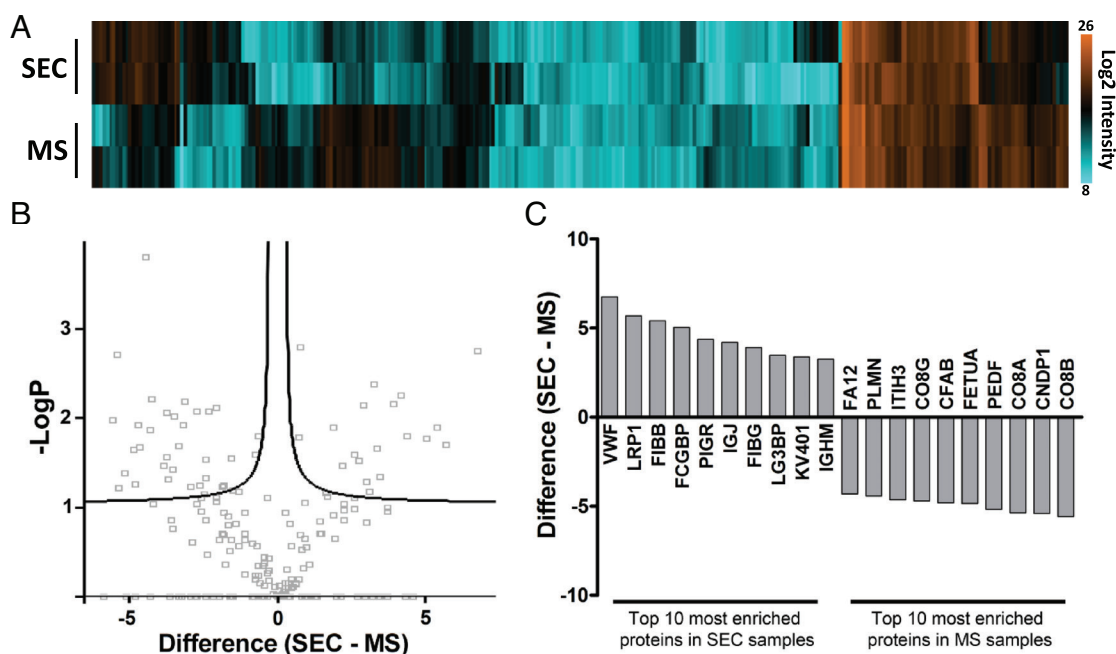
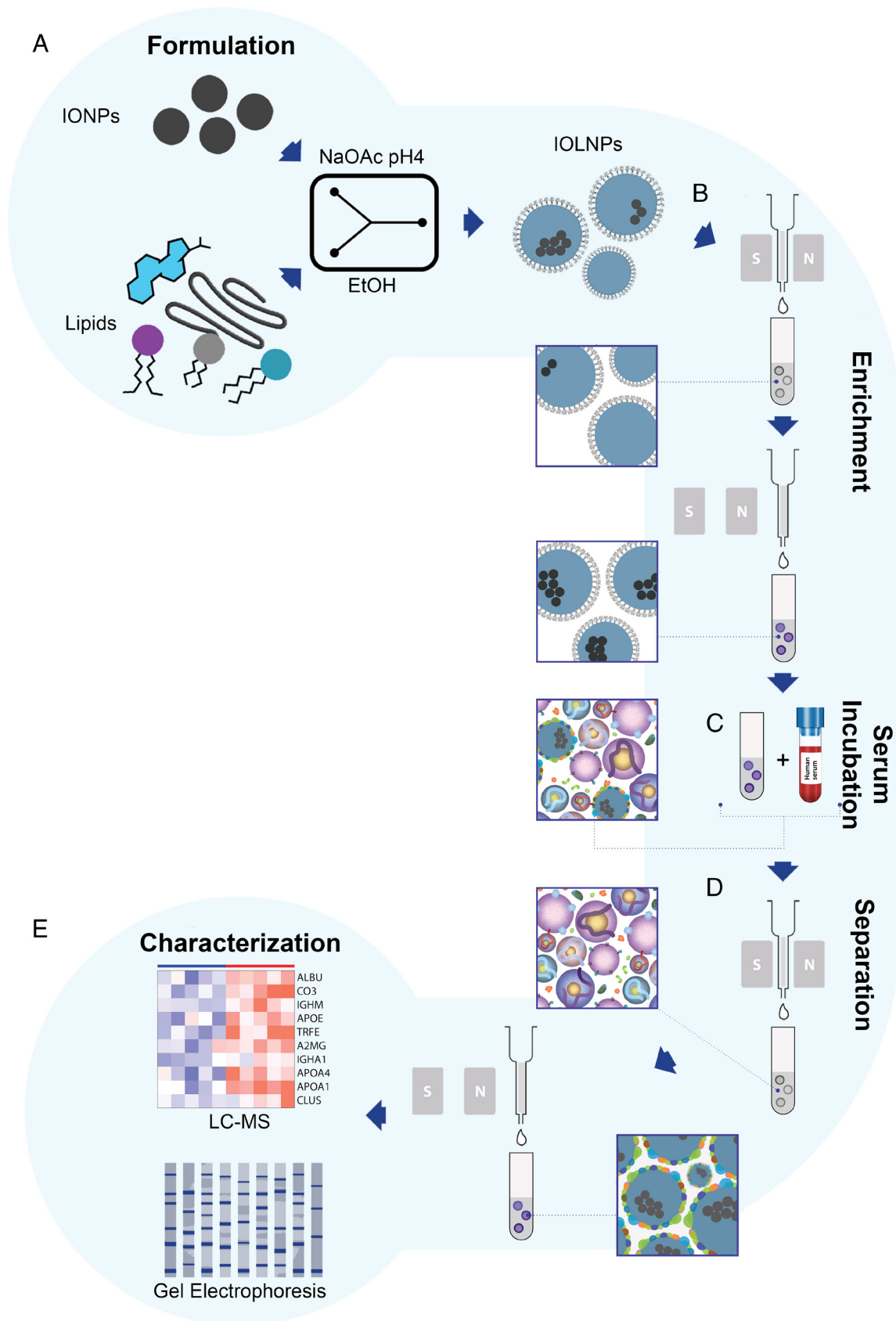


Fig. 4. Mass spectrometry data of IOLNP–corona complexes isolated by MS or SEC. IOLNPs were formulated and enriched as described in the *Materials and Methods*. The enriched IOLNPs were incubated in human serum for 1 h at 37 °C and then the 1 mL of human serum and IOLNPs was run through a magnetic (MS) or a SEC column. Samples were collected and the same protein amount was analyzed by LC–MS. (A) Heatmap analysis of the 200 proteins identified, in duplicate. Orange indicates the highest abundance while cyan indicates lower abundance. (B) Volcano plot representing the statistical difference in protein content between the 2 conditions (*t* test). x axis represents the difference between samples run via SEC or MS, with the highest values indicating that proteins (white dots) are more enriched in the SEC sample while the lowest values indicate that proteins are more enriched in MS samples. Values around zero indicate no difference. y axis shows how significant the difference in protein composition is, with the highest values being more significant. The two black lines represent the statistical cut-off considered in this analysis. Overall, 52 statistically different proteins were identified. (C) Of the 52 statistically different proteins identified shown in panel (C), here are reported the top 10 most enriched proteins in each sample and their gene names.



Scheme 1. Schematic representation of the experimental workflow. (A) Magnetic LNPs (IOLNPs) were formulated by rapid mixing lipids in ethanol with 5-nm iron oxide nanoparticles (IONPs) in an aqueous phase (sodium acetate at pH4) using a T-tube mixer. (B) The resulting formulation was run through a magnetic column placed into a magnetic separator: Empty LNPs or LNPs encapsulating low IONPs amounts were not retained in the column and washed away (Wash) while IOLNPs containing higher IONPs amounts were retained and subsequently eluted by removing the column from the magnetic stand (Elution). (C) The iron-enriched IOLNPs population was incubated in human serum for 1 h at 37 °C to form IOLNPs–corona complexes. (D) Samples were loaded into a magnetic column that retained only magnetic IOLNPs and their corona, while proteins and lipoproteins in excess were washed away. (E) The recovered IOLNPs–corona complexes were then analyzed by Coomassie blue staining and LC-MS.

protein profiles observed are more representative of the actual BMC experienced *in vivo*.

LNP technology is a state-of-the-art approach that is paving the way for the widespread use of LNP-based gene therapeutics including the COVID-19 messenger RNA (mRNA) vaccines (36). It is well established that the BMC can dramatically affect the tropism of LNPs as illustrated by the influence of adsorbed apo-E on uptake of Onpattro LNP into hepatocytes (4). Further, the binding of apo-E on the LNP surface can also lead to internal lipid rearrangement resulting in destabilization of the LNP core and promoting subsequent RNA release (37). However, detailed mechanisms behind the BMC of LNPs in relation to organ- or cell-specific gene delivery remains mostly unknown. Therefore, it is essential to improve our current understanding of the fundamental biological interaction between LNP and biological media in order to critically design the next generation of LNP for accessing and treating a wide range of diseases. Our study presents a robust method to isolate LNPs and their corona from complex media based on magnetism. We developed magnetic IOLNP by encapsulating IONPs in the LNP core. The MS technique using magnetic separator and magnetic column chromatography provides a rapid and reproducible tool for the separation of LNP–corona complexes from biological fluids and an in-depth characterization of its BMC with maintained particle integrity. Such method development is crucial in overcoming challenges posed by the analytical limitation of more conventional methods and provides new insight into the corona composition that may be masked by naturally abundant unbound protein as a result of artifacts that originated from the biological media.

Materials and Methods

LNP Formulation and Characterization. Lipids (DLin-MC3-DMA/DSPC/Cholesterol/PEG-DMG/DiDC18) were first dissolved in ethanol at a molar ratio of 50.0/10.0/38.5/1.5/0.5. Carboxylated IONPs (Ocean NanoTech, San Diego, CA) were resuspended in 25 mM sodium acetate buffer at pH4 at four different concentrations: 1.1×10^{13} , 2.2×10^{13} , 4.4×10^{13} , or 8.8×10^{13} IONP/ μ mol lipids. Formulations were prepared by rapid mixing the two phases using a T-junction mixer and a dual syringe pump (PHD Ultra, Harvard Apparatus, Holliston, MA) at a flow rate of 1:3 v/v (or 5 mL/min: 15 mL/min) of lipid: aqueous phase (27). The resulting suspension was dialyzed in PBS, sterile filtered using 0.2- μ m syringe filters, concentrated using 100 kDa Amicon Ultra centrifugal filters, and stored at 4 °C for up to 4 wk. siRNA-LNP control formulation was prepared using the same method and lipid composition with siRNA against luciferase (IDT, Coralville, IA) at an amine-to-phosphate ratio (N/P) of 3.

The particle hydrodynamic diameter, PDI, and size distribution were determined by dynamic light scattering (intensity mode; Zetasizer Nano ZS, Malvern Instruments Inc., Westborough, MA), using a disposable low volume plastic cuvette filled with IOLNPs diluted in PBS.

IOLNP content was measured using the Cholesterol E enzymatic assay kit (Wako Chemicals, Richmond, VA) to determine cholesterol concentration within the formulation from which the total lipid content was derived. Lipid concentration is calculated based on the initial weight percent of cholesterol that was employed within the formulation. A fluorescence assay was performed as a secondary method to determine IOLNP lipid content. Formulations containing the lipid dye DiDC18 were diluted 1:10 in PBS and 100 μ L was transferred into a 96-well black polystyrene plate. The fluorescence was measured at 590/645 nm (excitation/emission) with a sensitivity of 60 using a fluorescence plate reader (Dynex Technologies, Chantilly, VA).

Cryo-TEM imaging was performed at the UBC High Resolution Macromolecular Cryo-Electron Microscopy Facility (HRMEM) (Vancouver, BC). Samples were concentrated to approximately 20 mg/mL of total lipid using 100 kDa Amicon Ultra centrifugal filters. The average particle diameters and average number of IONPs of up to 100 randomly selected LNPs were manually measured using Fiji analysis software. Free IONPs were tabulated from wash and elution micrographs (14 frames each) across two independent experiments. Refer to *SI Appendix, Fig. S3D*

for representative images. The % free IONPs in wash or elution fraction was calculated using the equations below:

$$\frac{\text{Free IONPs in wash}}{\text{Free IONPs in wash} + \text{Free IONPs in elution}} \times 100\% \quad [1]$$

= % free IONPs in wash fraction,

$$\frac{\text{Free IONPs in elution}}{\text{Free IONPs in wash} + \text{Free IONPs in elution}} \times 100\% \quad [2]$$

= % free IONPs in elution fraction.

MS. MS was performed using a MACS® Cell Separation system composed of MidiMACS Separator, MultiStand, and LD or LS MACS Columns (Miltenyi Biotec Inc. Auburn, CA). Each column was primed by rinsing it 2 times with 3 mL PBS, followed by the addition of IOLNP formulation. The column was further washed twice with 3 mL PBS resulting in the collection of the flow through (wash fraction). Then, the cofractions removed from the magnet and magnetic stand and washed twice with 3 mL PBS to collect the elution fraction. Each fraction was then concentrated to approximately 500 μ L at 3,000 rpm using 100 kDa Amicon Ultra centrifugal filters. The concentrated solutions were then stored at 4 °C. When the MACS® Cell Separation system was used for corona studies, the elution fraction was concentrated further using 30 kDa Amicon Ultra 0.5-mL centrifugal filters to reach a volume of 25 to 30 μ L.

BMC Formation. Pooled gender 0.2- μ m sterile filtered human serum from at least 200 individuals was purchased from BioIVT (Westbury, NY) and stored at –20 °C. After thawing, 1 mL human serum was incubated at 37 °C for 1 h at 250 rpm with 94 μ g IOLNP total lipid/mL serum. The IOLNP/serum ratio was determined by using as a reference the injected Onpattro dose in the clinic (0.3 mg siRNA/kg or 3.3 mg total lipids/kg) and calculating the amount of serum in an average individual (2.63 L for 75 kg).

After incubation, 1 mL sample was loaded into a MACS® Cell Separation system (see above) or into a SEC column. For SEC, the sample was loaded into a 15 \times 1.5 cm column filled with Sepharose CL-4B (Sigma-Aldrich, Oakville, ON) and equilibrated with PBS. The eluate was collected in fractions of 0.5 mL and the absorbance of each fraction was measured at 280 nm on a NanoDrop Lite Spectrophotometer (ThermoFisher, Vancouver, BC). Fractions containing IOLNPs were pooled together and concentrated by using a 30 kDa Amicon Ultra centrifugal filter.

Protein concentration of samples separated by MACS® Cell Separation system or SEC was measured by Pierce™ BCA Protein Assay following the manufacturer's instructions (ThermoFisher, Vancouver, BC), while IOLNPs concentration was determined by fluorescence as described above.

Gel Electrophoresis. For sodium dodecyl sulfate (SDS) PAGE, samples were mixed with Laemmli sample buffer, boiled for 5 min at 95 °C, and loaded into a 4 to 15% Mini-PROTEAN® TGX™ Precast Protein Gel (Bio-Rad Laboratories Ltd. Mississauga, ON). After the electrophoretic run, the gel was incubated for 1 h with a solution containing 0.1% w/v Coomassie blue in MilliQ:methanol:glacial acetic acid (5:4:1). After overnight washes in MilliQ water, pictures were taken using a ChemiDoc.

For LC-MS analysis, 20 μ g protein for each sample was used. Protocol details can be found below.

In-Solution Digestion Protocol. The protein corona samples (20 μ g) were first diluted with 50 mM ammonium bicarbonate (pH ~ 8) for pH correction in a final volume of 50 μ L. Dithiothreitol (DTT) solution (0.5 μ g) was added to and incubated for 30 min at 37 °C to reduce the protein's disulfide bonds. Iodoacetamide solution (2.5 μ g) was then added and incubated for 20 min at 37 °C in the dark to block free sulfhydryl groups. Trypsin solution (0.5 μ g) was added and incubated for 20 h at 37 °C. Subsequently, quenching of trypsin activity was achieved by sample acidification through the addition of 1% trifluoroacetic acid (TFA) until a pH < 2.5 was obtained and then cleaned up via STAGE-Tip purification. Samples were passed through a primed and equilibrated C18 column (14 mm), washed twice with aqueous phase 1% TFA, and eluted into organic phase containing 40% acetonitrile (ACN) and 0.1% TFA. The resulting sample was then dried down.

Mass Spectrometry Analysis. Reconstituted samples in 2% ACN and 0.5% formic acid, and protein corona samples were analyzed using an EasyLC 1000 HPLC (ThermoFisher Scientific) equipped with a Captive spray nanospray ionization source (Bruker Daltonics) and protein corona samples were detected with a quadrupole-time-of-flight (QD-TOF) mass spectrometer (Impact II; Bruker Daltonics). An Aurora Series Gen2 (CSI) analytical column (25 cm × 75 μm 1.6 μm FSC C18, with Gen2 nanoZero and CSI fitting; Ion Opticks, Parkville, Australia), and a μ-Pre-column (300 μm ID × 5 mm, C18 PepMap, 5 μm, 100 Å, Thermo Scientific, Waltham, MA) was used for the HPLC separation. The analytical column was heated to 50 °C during the separation using a tape heater (SRMU020124, Omega.com) and an in-house build microprocessor temperature controller.

Buffers A and B were composed of 0.1% aqueous formic acid with 2% ACN in water (aqueous phase) and 0.1% formic acid in 90% ACN (organic phase), respectively. Samples were reconstituted and loaded in buffer A. For a standard 90-min run, the gradient B was programmed to go from 5 to 18% over 45 min, then to 35% from 45 to 90 min, then to 90% over 2 min, and held at 90% for 13 min. Before each run, buffer A was used to condition the analytical column (4 μL) and pre-column (20 μL). The LC thermostat temperature was programmed at 7 °C with the analysis operating at a flowrate of 0.35 μL/min. OTOF Control v. 4.1 (Bruker) was used to run Impact II. LC and MS were controlled with HyStar 4.1 (4.1.21.2, Bruker). The acquisition of the Impact II was programmed in a data-dependent auto-MS/MS mode with inactive focus fragmenting the 20 most abundant ions (at 18 Hz rate) after each full-range scan from m/z 200 Th to m/z 2,000 Th (at 5 Hz rate). The isolation window for MS/MS was 2 to 3 Th as determined by the parent ion's mass-to-charge ratio with the collision energy ranging from 23 to 65 eV based on ion mass and charge. For the next 0.3 min, parent ions were excluded from MS/MS and reevaluated if their intensity increased more than fivefold. As ESI mode protein generally carry multiple charges, singly charged ions were excluded.

Proteomic Search. Acquired data were then searched against the UniprotKB protein database for Homo sapiens using the software MaxQuant. The search was

performed using 20 ppm and 40 ppm mass accuracies for precursor and product ion masses, respectively, and a 1% false discovery rate cut-off.

Statistical Analysis. Comparisons were made between distinct groups. Groups were analyzed by two-tailed unpaired *t* test. Statistical significance was set as **P* < 0.05 and ***P* < 0.01, with a 95% CI. Analysis and figures were generated using GraphPad Prism v. 7.0 and 9.0.

Data, Materials, and Software Availability. All study data are included in the article and/or *SI Appendix*.

ACKNOWLEDGMENTS. We acknowledge the support from the Canadian Institutes for Health Research (FDN 148469), the NanoMedicines Innovation Network (NMIn), a Canadian Networks of Centres of Excellence in nanomedicine, and the European Union's Horizon 2020 research and innovation programme "EXPERT" (#825828). Y.Z. acknowledges the funding from the University of British Columbia Faculty of Medicine program. D.W. is supported by the Swiss NSF (#183923). M.H.Y.C. is funded by NMIn postdoctoral fellowship in gene therapy. Mass spectrometry analysis was performed in the mass spectrometry facility of the faculty of medicine at the University of British Columbia. We would like to thank Jason Rogalski for his technical support and suggestions. Graphic content was implemented by V.F. with the help of Miltenyi Biotec. Grids were prepared and data collected at the High Resolution Macromolecular Electron Microscopy (HRMEM) facility at the University of British Columbia (<https://cryoem.med.ubc.ca/>). We thank Claire Atkinson, Joseph Felt, Liam Worrall and Natalie Strynadka. HRMEM is funded by the Canadian Foundation of Innovation and the British Columbia Knowledge Development Fund.

Author affiliations: ^aDepartment of Biochemistry and Molecular Biology, University of British Columbia, Vancouver, BC V6T 1Z3, Canada; ^bDepartment of Clinical Chemistry and Haematology, University Medical Center Utrecht, Utrecht 3584, Netherlands; and ^cNanoVation Therapeutics, Vancouver, BC V6T 1Z3, Canada

1. J. A. Kulkarni, D. Witzigmann, S. Chen, P. R. Cullis, R. Van Der Meel, Lipid nanoparticle technology for clinical translation of siRNA therapeutics. *Acc. Chem. Res.* **52**, 2435–2444 (2019).
2. D. Witzigmann *et al.*, Lipid nanoparticle technology for therapeutic gene regulation in the liver. *Adv. Drug Deliv. Rev.* **159**, 344–363 (2020).
3. J. Buck, P. Grossen, P. R. Cullis, J. Huwyler, D. Witzigmann, Lipid-based DNA therapeutics: Hallmarks of non-viral gene delivery. *ACS Nano* **13**, 3754–3782 (2019).
4. A. Akinc *et al.*, Targeted delivery of RNAi therapeutics with endogenous and exogenous ligand-based mechanisms. *Mol. Ther.* **18**, 1357–1364 (2010).
5. D. Adams *et al.*, Patisiran, an RNAi therapeutic, for hereditary transthyretin amyloidosis. *N. Engl. J. Med.* **379**, 11–21 (2018).
6. A. Akinc *et al.*, The Onpatro story and the clinical translation of nanomedicines containing nucleic acid-based drugs. *Nat. Nanotechnol.* **14**, 1084–1087 (2019).
7. J. A. Kulkarni *et al.*, The current landscape of nucleic acid therapeutics. *Nat. Nanotechnol.* **16**, 630–643 (2021).
8. E. Samaridou, J. Heyes, P. Lutwyche, Lipid nanoparticles for nucleic acid delivery: Current perspectives. *Adv. Drug Deliv. Rev.* **154–155**, 37–63 (2020).
9. C. Horejs, From lipids to lipid nanoparticles to mRNA vaccines. *Nat. Rev. Mater.* **6**, 1075–1076 (2021).
10. M. Torrice, Does nanomedicine have a delivery problem? *ACS Cent. Sci.* **2**, 434–437 (2016).
11. S. Hua, M. B. C. De Matos, J. M. Metselaer, G. Storm, Current trends and challenges in the clinical translation of nanoparticulate nanomedicines: Pathways for translational development and commercialization. *Front. Pharmacol.* **9**, 790 (2018).
12. H. H. Gustafson, D. Holt-Casper, D. W. Grainger, H. Ghandehari, Nanoparticle uptake: The phagocytosis problem. *Nano Today* **10**, 487–510 (2015).
13. K. Paunovska *et al.*, A direct comparison of in vitro and in vivo nucleic acid delivery mediated by hundreds of nanoparticles reveals a weak correlation. *Nano Lett.* **18**, 2148–2157 (2018).
14. G. Caraciolo *et al.*, Selective targeting capability acquired with a protein corona adsorbed on the surface of 1,2-dioleoyl-3-trimethylammonium propane/DNA nanoparticles. *ACS Appl. Mater. Interfaces* **5**, 13171–13179 (2013).
15. M. Papi *et al.*, Clinically approved PEGylated nanoparticles are covered by a protein corona that boosts the uptake by cancer cells. *Nanoscale* **9**, 10327–10334 (2017).
16. Y. Zhang, J. L. Y. Wu, J. Lazarovits, W. C. W. Chan, An analysis of the binding function and structural organization of the protein Corona. *J. Am. Chem. Soc.* **142**, 8827–8836 (2020).
17. D. Chen, N. Parayath, S. Ganesh, W. Wang, M. Amiji, The role of apolipoprotein- and vitronectin-enriched protein corona on lipid nanoparticles for in vivo targeted delivery and transfection of oligonucleotides in murine tumor models. *Nanoscale* **11**, 18806–18824 (2019).
18. S. Morita, A. Sakurai, M. Nakano, S. Kitagawa, T. Handa, Presence of apolipoprotein C-III attenuates apolipoprotein E-mediated cellular uptake of cholesterol-containing lipid particles by HepG2 cells. *Lipids* **46**, 323–332 (2011).
19. V. Francia, R. M. Schifflers, P. R. Cullis, D. Witzigmann, The biomolecular corona of lipid nanoparticles for gene therapy. *Bioconj. Chem.* **31**, 2046–2059 (2020).
20. T. Nakamura *et al.*, Extrahepatic targeting of lipid nanoparticles in vivo with intracellular targeting for future nanomedicines. *Adv. Drug Deliv. Rev.* **188**, 114417 (2022).
21. S. A. Dilliard, Q. Cheng, D. J. Siegwart, On the mechanism of tissue-specific mRNA delivery by selective organ targeting nanoparticles. *Proc. Natl. Acad. Sci. U.S.A.* **118**, e2109256118 (2021).
22. M. Qiu *et al.*, Lung-selective mRNA delivery of synthetic lipid nanoparticles for the treatment of pulmonary lymphangioliomyomatosis. *Proc. Natl. Acad. Sci. U.S.A.* **119**, e2116271119 (2022).
23. V. Francia *et al.*, Corona composition can affect the mechanisms cells use to internalize nanoparticles. *ACS Nano* **13**, 11107–11121 (2019).
24. R. Pattipeiluhu *et al.*, Unbiased identification of the liposome protein corona using photoaffinity-based chemoproteomics. *ACS Cent. Sci.* **6**, 535–545 (2020).
25. M. Zhou *et al.*, Effective lock-in strategy for proteomic analysis of corona complexes bound to amino-free ligands of gold nanoparticles. *Nanoscale* **10**, 12413–12423 (2018).
26. F. Sebastiani, M. Yanez Arteta, L. Lindfors, M. Cárdenas, Screening of the binding affinity of serum proteins to lipid nanoparticles in a cell free environment. *J. Colloid Interface Sci.* **610**, 766–774 (2022).
27. A. K. Leung, Y. Y. C. Tam, S. Chen, I. M. Hafez, P. R. Cullis, Microfluidic mixing: A general method for encapsulating macromolecules in lipid nanoparticle systems. *J. Phys. Chem. B* **119**, 8698–8706 (2015).
28. K. Bromma *et al.*, Use of a lipid nanoparticle system as a Trojan horse in delivery of gold nanoparticles to human breast cancer cells for improved outcomes in radiation therapy. *Cancer Nanotechnol.* **10**, 1 (2019).
29. J. A. Kulkarni *et al.*, On the formation and morphology of lipid nanoparticles containing ionizable cationic lipids and siRNA. *ACS Nano* **12**, 4787–4795 (2018).
30. M. Hadjidemetriou, Z. Al-Ahmady, K. Kostarelou, Time-evolution of in vivo protein corona onto blood-circulating PEGylated liposomal doxorubicin (DOXIL) nanoparticles. *Nanoscale* **8**, 6948–6957 (2016).
31. M. P. Monopoli, S. Wan, F. B. Bombelli, E. Mahon, K. A. Dawson, Comparisons of nanoparticle protein corona complexes isolated with different methods. *Nano LIFE* **03**, 1343004 (2013).
32. T. Cedervall *et al.*, Understanding the nanoparticle-protein corona using methods to quantify exchange rates and affinities of proteins for nanoparticles. *Proc. Natl. Acad. Sci. U.S.A.* **104**, 2050–2055 (2007).
33. Y. Yuana *et al.*, Cryo-electron microscopy of extracellular vesicles in fresh plasma. *J. Extracell. Vesicles* **2**, 21494 (2013).
34. E. Chekol Abebe *et al.*, The structure, biosynthesis, and biological roles of fetuin-A: A review. *Front. Cell Dev. Biol.* **10**, 945287 (2022).
35. J. B. Simonsen, R. Münter, Pay attention to biological nanoparticles when studying the protein corona on nanomedicines. *Angew. Chem. Int. Ed. Engl.* **59**, 12584–12588 (2020).
36. M. H. Y. Cheng, C. A. Brimacombe, R. Verbeke, P. R. Cullis, Exciting times for lipid nanoparticles: How Canadian discoveries are enabling gene therapies. *Mol. Pharm.* **19**, 1663–1668 (2022).
37. F. Sebastiani *et al.*, Apolipoprotein E binding drives structural and compositional rearrangement of mRNA-containing lipid nanoparticles. *ACS Nano* **15**, 6709–6722 (2021).